

Liquid Crystals

The Special “Morse Code” between Solvent Polarity and Morphology Flexibility in a POSS–Dendrimer Supramolecular System**

Tianyu Shan^{+, [a]} Liang Gao^{+, [b]} Xiaoqian Tong,^[a] Qinqing Du,^[a] Zhihang An,^[a] Huiwen He,^[a] Jiaping Lin,^{*, [b]} Si Chen^{+, * [a]} and Xu Wang^{*, [a]}

Abstract: An amazing phenomenon of the relative magnitude of modulus of two liquid-crystal (LC) gels is found inverted under/above their phase transition temperature T_{LC-iso} which is further proved to be caused by their diverse morphology flexibility. By testing the polarity of two LCs, gelator POSS-G1-Boc (POSS = polyhedral oligomeric silsesquioxane) was discovered to self-assemble into more flexible structures in a relatively low polar LC, whereas more rigid ones are

formed in higher polar LC. Hence, a fitting function to connect morphology flexibility with solvent polarity was established, which can even be generalized to a number of common solvents. Experimental observations and coarse-grained molecular dynamics simulations revealed that solvent polarity mirrors a “Morse code”, with each “code” corresponding to a specific morphology flexibility.

Introduction

Liquid crystal (LC) physical gels are a new class of dynamically functional materials consisting of LCs and fibrous aggregates of molecules that are called “gelators”,^[1–3] which exhibit induced or enhanced electro-optical,^[4–6] photochemical,^[7,8] and electronic properties.^[9–10] Phase-separated structures are formed in LC physical gels by the combination of two components, which can further affect the photoelectric performance due to the change of interface action on the boundary regions.^[11–13] Hence the regulation of various morphologies of LC gel is crucial.

Research on the morphology of LC gels has concentrated on situations in which the sol-gel transition temperature $T_{sol-gel}$ is higher than the phase-transition temperature T_{LC-iso} and Kato's work^[14] points out that aligned fibers are formed by the tem-

plate effects of oriented LCs in this case. In contrast, randomly dispersed networks are formed in the isotropic phase when $T_{sol-gel}$ is lower than T_{LC-iso} . In fact, our research reveals that the morphology is affected by the diverse LCs even though the gelators self-assemble in an isotropic phase, which is caused by the strong interaction force between gelators and LC molecules. That is to say, as an absolute majority part in the gel system, solvents do have unignorable effects on the resultant assembly of nanostructures due to the substantial interactions between solvents and gelators. Hence, in our supramolecular system, we can regard LCs as general solvents, and neglect their orientational ordering nature.



In Q. Jin's research,^[15] the same gelator molecule can self-assemble into diverse nanostructures over a wide scale range from nanofibers, nanotwists, to nanotubes and microtubes in different solvents, depending on the solvent polarity and their hydrogen-bonding nature. Nevertheless, research on solvent-induced morphology has always focused on common solvents rather than the LCs,^[16–22] which may be due to the lack of knowledge of LCs solvent parameters. Herein, by measuring the solvent polarity of LCs and quantitatively comparing fiber flexibility, we connect solvent polarity with morphology flexibility by a fitting function, which can even be generalized to some common solvents. Furthermore, additional coarse-grained molecular dynamics simulations unambiguously support our theory that the solvent polarity is just like the special “Morse code”, and the special “code” can be decoded as morphology flexibility by the fitting function we built. We hope it could provide a quick way to judge morphology flexibility before conducting cost- and time-consuming electron microscopy studies in analogous POSS-dendrimer supramolecular systems.

[a] T. Shan,⁺ X. Tong, Q. Du, Z. An, H. He, Prof. S. Chen,⁺ Prof. X. Wang
College of Materials Science and Engineering
Zhejiang University of Technology
Hangzhou 310014 (China)
E-mail: chensi@zjut.edu.cn
wangxu@zjut.edu.cn

[b] L. Gao,⁺ Prof. J. Lin
Shanghai Key Laboratory of Advanced Polymeric Materials
School of Materials Science and Engineering
East China University of Science and Technology
Shanghai 200237 (China)
E-mail: jlin@ecust.edu.cn

[†] These authors contributed equally to this work.

[**] POSS = polyhedral oligomeric silsesquioxane.

 Supporting information and the ORCID identification number(s) for the author(s) of this article can be found under:
 <https://doi.org/10.1002/chem.201901422>.

Results and Discussion

The gelator used in this study has a polyhedral oligomeric silsesquioxane (POSS) core with eight spatially symmetric lysine derivative "arms", named POSS-G1-Boc (Figure 1). The synthesis, characterization and self-assembly mechanism of POSS-G1-Boc in diverse organic solvents are discussed thoroughly in previous reports.^[23–25] The cubic structure of the inorganic POSS core meant that the gelator underwent plane-to-plane stacking and ultimately formed a loofah-like network which was supported by a sectional type hexagonal columnar assembly mode rather than physical entanglement of the length-limited fibers (Scheme S1 in the Supporting Information). In this paper, the gelator POSS-G1-Boc was introduced to LCs 4'-pentyl-4-biphenylcarbonitrile (5CB) and 4'-octyl-4-biphenylcarbonitrile (8CB); their chemical structures and that of POM are given in Figure 1 and Figure S1 (Supporting Information).

As a basic measurement of LC gels, it was surprising to find that the relative magnitude of modulus of two LC gels is inverted under/above the phase-

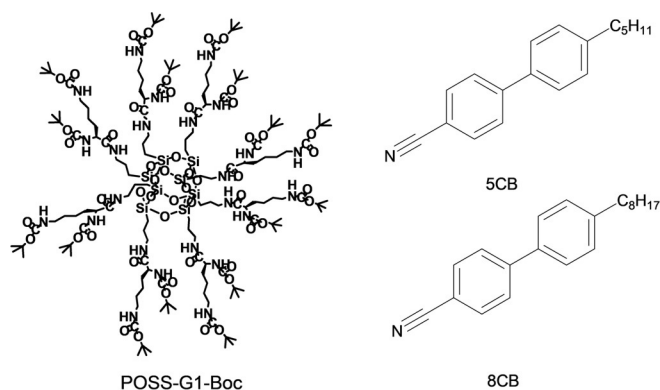


Figure 1. Chemical structures of LCs 5CB, 8CB and gelator POSS-G1-Boc.

transition temperature T_{LC-iso} (a phase diagram of LC gels is shown in Figure 2a). To be specific, 8CB gels have higher modulus than 5CB gels at room temperature (below the T_{LC-iso}), whereas the modulus of 5CB gels are higher at 50 °C (above the T_{LC-iso}), as clearly shown in Figure 2b,c. Given that it has been shown that pure LC 8CB has higher modulus than 5CB when both are below the T_{LC-iso} (Figure 2b), which is caused by more intense intermolecular forces of 8CB, it is not puzzling to understand that 8CB gels has a higher modulus under the circumstances. However, the underlying reasons for the inversion of rheological properties when above T_{LC-iso} are not yet clear.

It has been reported that molecular packing is the primary reason for the distinction of gelling abilities such as rheological properties.^[26] However, XRD patterns (Figure 2d) show that there is no evident distinction in molecular packing, and well-defined patterns indicate hexagonal columnar packing exist in both LC gels. Table 1 shows three major diffraction peaks of

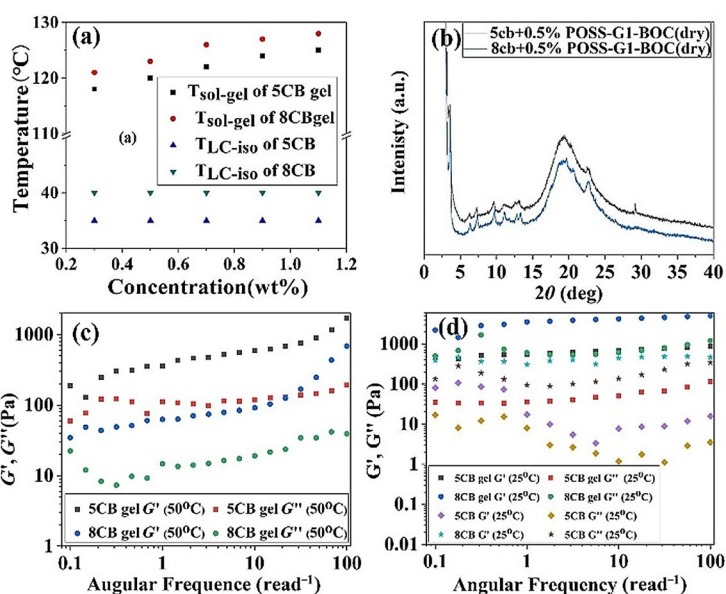


Figure 2. a) Phase diagram of two LCs and two LC gels; Rheological measurement of two LCs and LC gels with 0.1% strain, at temperatures of b) 25 °C; c) 50 °C. d) The XRD figure of two LC xerogel, indicating hexagonal columnar packing.

Table 1. The d -spacings [Å] of two LC xerogels calculated from XRD.

	P ₁	P ₂	P ₁ '	P ₃	P ₁ ''	P ₂ '	P ₃ '
5CB xerogel	24.94	14.10	12.14	9.17	7.99	6.77	4.66
8CB xerogel	24.39	13.89	12.03	9.06	7.97	6.74	4.48

5CB and 8CB xerogels P₁, P₂, and P₃, corresponding to d -spacings of 24.94, 14.10, 9.17 Å and 24.39, 13.89, 9.06 Å respectively. The d values which are in the ratio of $1:1/\sqrt{3}:1/\sqrt{7}$ can be reasonably indexed as the (100), (110), (210) diffractions. P₁', P₂' and P₃' with values of 12.14, 6.77, 4.66 Å and 12.03, 6.74, 4.48 Å, respectively, were assigned to the second-order diffractions of (100), (110) and (210). P₁'' was ascribed to the third-order diffraction of (100) with d values of 7.99 and 7.97 Å. Therefore, POSS-G1-Boc is supposed to form a hexagonal columnar structure in both 5CB and 8CB with a column diameter of 28.7 Å and 28.1 Å, respectively.

Considering that the self-assembly mechanism of gelators involves initial formation of microscopic fibers based on non-covalent bonds, then for gels based on an intertwined three-dimensional network,^[27–29] we could assume that the inversion of rheological properties is likely to happen on the fiber level since at the molecule level there seems to be no difference between 5CB and 8CB gel systems.

We therefore studied the microscopic morphology by soaking LC gels in *n*-hexane to remove LC. Figure 3 shows that three-dimensional networks have been formed by the LC, which prevent them from flowing. Furthermore, left-handed helical fibers can be found in both 5CB gel and 8CB gel, which will be examined in more detail in subsequent studies. Fibers with diverse flexibility can be found between two LC xerogels.

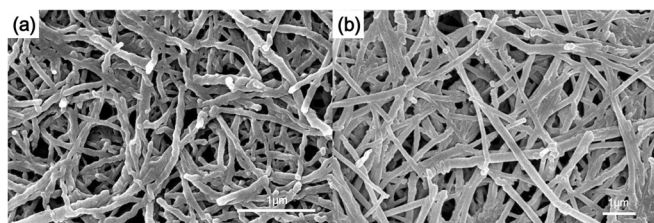


Figure 3. SEM images of a) 5CB and b) 8CB xerogels, LCs are removed with *n*-hexane. Fibers with diverse flexibility can be found.

More specifically, fibers in 5CB were more flexible, whereas 8CB make them more rigid. As $T_{\text{sol-gel}}$ is higher than $T_{\text{LC-iso}}$ for both LC gels (Figure 1 a), gel fibers are formed in isotropic solvents, so the LC phases will not influence the morphology flexibility (Figure S2). Given that flexible fiber networks are more effective at forming potent networks, which can be more clearly seen in extreme circumstances in Figure 4 a, it is clearly the critical factor that causes the unique inversion of rheological properties.

Therefore, what actually caused the diverse morphology of two LC gels? Figure 1 a shows that the $T_{\text{sol-gel}}$ is higher than $T_{\text{LC-iso}}$ for both LC gels, indicating that these fibers form an isotropic phase, which clearly suggests that it is not the common sense idea that people used to think of as two LC phases with diverse anisotropic ordered structures that play the key role.

Since gelator POSS-G1-Boc self-assembled in an isotropic phase, LCs could be considered as novel types of solvents. From the point of view of the mechanism of self-assembly, the polarity of the solvent significantly influences the morphology because of the interactions between solvents and gelators. Unfortunately, as uncommon solvents, the polarities of 5CB and 8CB are unknown; hence, we tested the normalized Reichardt's parameter E_T^N of these LCs to characterize polarity (see the Experimental Section). Figure S3 (Supporting Information) shows that the λ_{max} (the maximum absorption wavelength of Reichardt's dye) of 5CB and 8CB are 736 and 710 cm^{-1} , respectively, hence the E_T^N values can be calculated as 0.25 and 0.3, respectively, by using Equation (1),^[30] which suggests POSS-G1-Boc can form flexible fibers in low E_T^N value solvents and rigid fibers in high E_T^N value solvents. Given that the POSS core of POSS-G1-Boc is nonpolar, and the recognition of the POSS core always comes first by hydrophobic force in the self-assembly process,^[23] we speculate that solvents with high E_T^N value facilitates the hydrophobic POSS core self-assembly into one-dimensional fibers by hydrophobic interactions, ultimately resulting in microscopic rigid fibers (Scheme 1).

For the next step, it is quite natural to wonder whether the model can be used to predict the morphology induced by various solvents; hence, we selected a range of solvents with various E_T^N values to address this question. Cyclohexane, *N,N*-dimethylcyclohexylamine, 1,2-dimethoxyethane, and acetonitrile

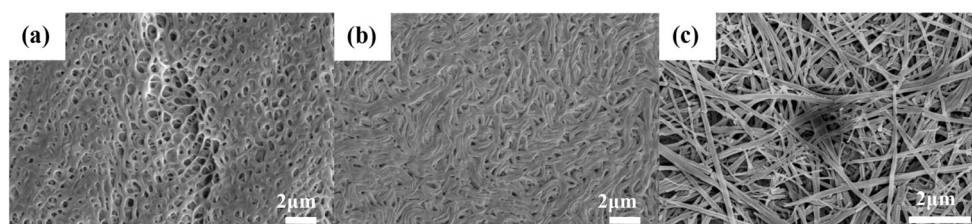
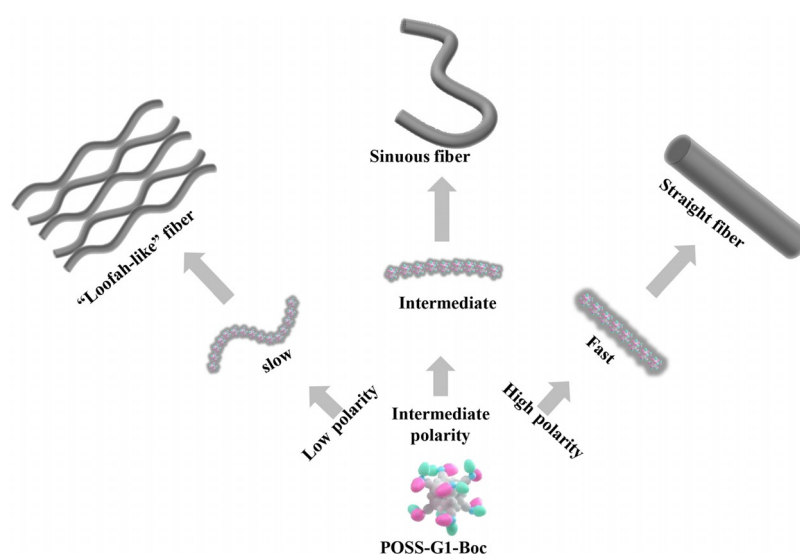


Figure 4. Morphologies of samples with diverse fiber flexibility self-assembled in a) *N,N*-dimethylcyclohexylamine; b) 1,2-dimethoxyethane and c) acetonitrile.



Scheme 1. A schematic showing how gelator POSS-G1-Boc forms flexible fibers in diverse polar solvents.

were chosen because of their broad scope from low to high E_T^N values (Table S1, Supporting Information). Considering that they are conventional solvents, their E_T^N can be calculated by hydrogen-bond donating ability α and polarizability π^* by using Equation (1) and Equation (2) (the values of α and π^* can be obtained in the literature).^[30] Figure 4 shows that *N,N*-dimethylcyclohexylamine with low E_T^N value of 0.10 forms flexible “loofah-like” morphology (Figure 4a), 1,2-dimethoxyethane with intermediate value of 0.20 forms sinuous fibers without any branching (Figure 4b), and rigid rod-like fibers (Figure 4c) are formed in acetonitrile with high E_T^N value of 0.36; these results are completely in accordance with the model described above, indicating ideal verification of our model. More surprisingly, intermediate flexible sinuous fibers occur when a mixed solvent system of *N,N*-dimethylcyclohexylamine and acetonitrile with equal volume proportion was used (Figure S4, Supporting Information). Furthermore, precipitation occurred when the lowest E_T^N value solvent cyclohexane was used, because of the low solubility of gelator POSS-G1-Boc in this solvent. That is to say, E_T^N is just like the special “Morse code”, and each value of E_T^N corresponds to a specific fiber flexibility.

$$E_T^N = \frac{(28591/\lambda_{\max}) - 30.7}{32.4} \quad (1)$$

$$E_T = \frac{\alpha + 0.72\pi^* + 2.03}{0.0649} \quad (2)$$

$$E_T^N = \frac{E_T - 30.7}{32.4}$$

To quantitatively compare the flexibility of different fibers, we define a new parameter X to characterize fiber flexibility as follows: going forward along the fiber from a point for 1 μm , and X defined as the straight-line distance to origin (Figure 5a). Especially for the “loofah-like” morphology, X should be amended as the vector sum of each branch (Figure 5b). Apparently, fibers with larger X values have less flexibility. Utilizing the parameter X , we can read the special “Morse code” E_T^N by a fitting function (Figure 6), which provided good correlation of the X value with E_T^N . Clearly, parameter X shows a positive correlation with “Morse code” E_T^N , which means fiber flexibility decreases with increasing solvent polarity. Then, with the help of the “decoding tool”- the fitting function, we are able to read the special “Morse code” E_T^N in all values.

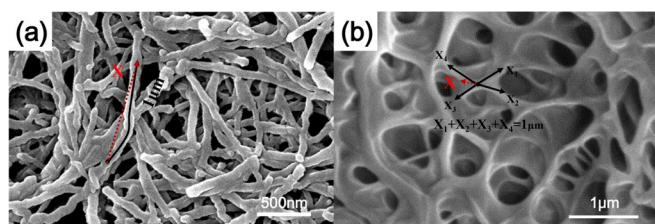


Figure 5. The method of the parameter X defined. The black full lines indicate the route along the fiber from a point for 1 μm , and the red dash line indicates the straight-line distance (X) to origin.

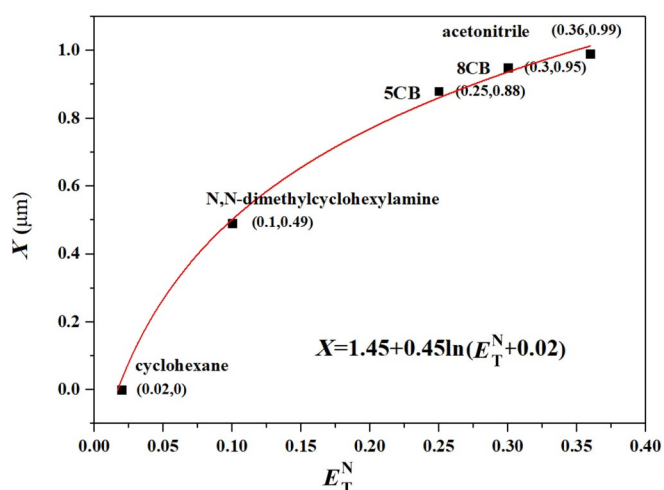


Figure 6. The figure of fitting function, connecting polarity parameter E_T^N with fiber flexibility parameter X .

To further reveal the effect of solvent polarity on fibrous morphologies and to verify the mechanisms proposed above, we performed coarse-grained molecular dynamics simulations on the assembly of POSS-G1-Boc in the polar solvent. As shown in Figure 7a, we first built a coarse-grained molecular

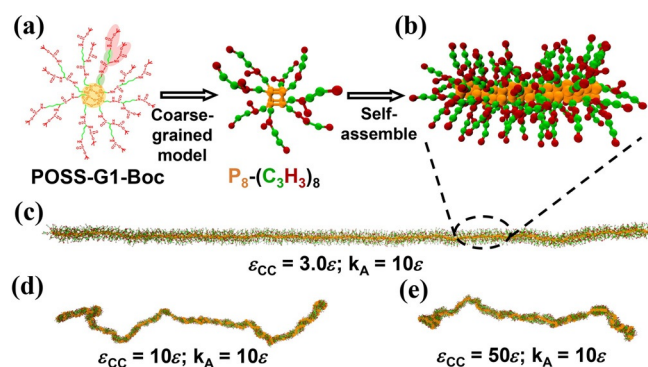


Figure 7. a) Coarse-grained model and mapping relationship. b) Partial enlarged detail of fibrous morphologies. c–e) Simulation snapshots of aggregate morphologies formed at various interaction parameters: c) $\epsilon_{CC} = 3.0\epsilon$, $k_A = 10\epsilon$; d) $\epsilon_{CC} = 10\epsilon$, $k_A = 10\epsilon$; e) $\epsilon_{CC} = 3.0\epsilon$, $k_A = 10\epsilon$.

model $P_8-(C_3H_3)_8$ for POSS-G1-Boc, in which P (orange beads), C (green beads) and H (red beads) represent the POSS cube, the tether carbon chain, and the functional group which can form the hydrogen bond, respectively. Different potential functions between the pair of beads were chosen to describe the solvophobic nature and the hydrogen-bond interaction of POSS-G1-Boc (details of model and method are given in the Experimental Section).

To simulate the formation of fibrous morphologies in a polar solvent, the strength k_A of hydrogen-bond interaction between H beads was set as 10ϵ , and the strength of solvophobic interaction for P and C beads was set as $\epsilon_{PP} = 10\epsilon$, and $\epsilon_{CC} = 3.0\epsilon$. With simulation time, $P_8-(C_3H_3)_8$ first assembles into short cylindrical aggregates, and then end-to-end connects with each other to form straight fibrous aggregates (Figure 7c and Fig-

ure S5, Supporting Information). The partial enlarged detail (Figure 7b) indicated that the POSS cubes are orderly packed to form the core of fibrous aggregates, while the tethered chains make up the corona that evenly surrounds the POSS core. In the experimental observations, with decreasing polarity of solvent, the fibrous morphologies become increasingly flexible and sinuous. According to the variations of the Kamlet–Taft parameters (Table S1, Supporting Information), the decrease of polarity (i.e., the value of E_T^N) is mainly reflected in the lower π^* values, resulting in a poorer solubility of polar tethered chains. Given the minor variations of the values of α in the Kamlet–Taft parameters with decreasing polarity, the hydrogen-bond interaction is maintained unchanged. In addition, the inorganic POSS cubes have a poor solubility and they tend to aggregate in organic solvent. Thus, in a less polar solvent, the polar tethered chains (C beads) are more solvophobic.

Corresponding to the aggregation behavior in a less polar solvent, the interaction parameter ϵ_{CC} gradually increased to 10ϵ , 25ϵ and 50ϵ , and the morphologies transformed from straight fiber into curved and sinuous fiber (Figure 7d,e). Notably, the corona formed by the tethered chains collapsed on the POSS core, and showed an uneven distribution in the less polar solvent. Such a collapsing variation can minimize the surface energy between tethered chains and solvents, while the solvophobic POSS segments maintain aggregation in the core. Therefore, with decreasing polarity of solvent, the fibrous aggregates curved to adopt more flexible morphologies.

To further examine the variation of fibrous morphologies, an unperturbed dimension A_f of fiber structures was defined according to the definition of unperturbed dimension, which describes the flexibility of the polymer chains.^[31] As shown in Figure 8, A_f was obtained from the ratio of the terminal distance h between two fiber ends to the square root of the number N of $P_8-(C_3H_3)_8$ in the aggregates. The values of A_f of the simulation morphologies at various interaction parameter ϵ_{CC} was calculated and shown in Figure 8. The result indicates that the unperturbed dimension A_f of fiber structures gradually

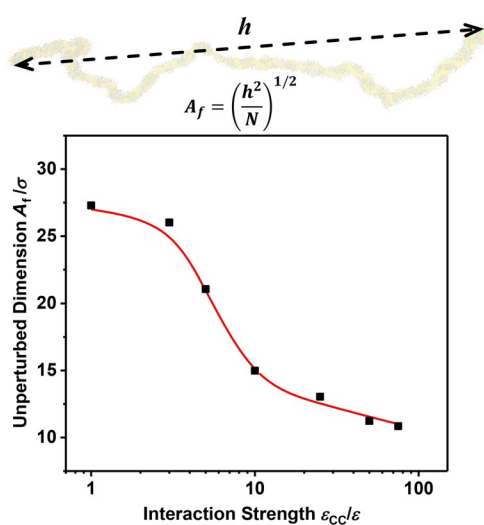


Figure 8. Variation of unperturbed dimension A_f with increasing interaction strength ϵ_{CC} .

decrease with increasing ϵ_{CC} , which is consistent with the experimental observations. Therefore, the polarity of solvent plays a significant role in the flexibility of fibrous morphologies, and further determines the structure and properties of the gel network.

Conclusions

We have discovered that the morphology flexibility of LC gels is affected by LC molecules, although the gelators self-assemble in an isotropic phase. The law can be extended to ecumenical organic solvents in accordance with their polarity nature: gelator POSS-G1-Boc can self-assemble into one-dimensional fibers more easily in high polar solvents by hydrophobic interactions, ultimately resulting in more rigid microscopic fibers. The results were verified by coarse-grained molecular dynamics simulations. With the help of special “Morse code” E_T^N , we link the morphology with polarity together, allowing the morphology flexibility to be rapidly estimated before electron microscope measurements are conducted.

Experimental Section

Materials: LCs 5CB and 8CB were purchased from Yantai Valiant Fine Chemicals Co., Ltd. *N,N*-dimethylcyclohexylamine and acetonitrile were supplied by Aladdin (China) Chemical Co., Ltd. The gelators POSS-G1-Boc were synthesized in our laboratory.

Preparation of LC physical gels and xerogels: A certain amount of POSS-G1-Boc were dissolved into LCs at 155°C to form LC physical sol, and LC physical gels were prepared by cooling the sol to 25°C in air. After aging at 25°C for 30 min, the LC gels were soaked in *n*-hexane for two days to remove LCs. The LC xerogel suspension liquid was then dropped on a silicon wafer, followed by removal of the remaining *n*-hexane under vacuum at 25°C . Other ecumenical organic xerogels were prepared by conventional freeze-drying to reduce the effect of solvent evaporation on the morphology. The concentration of gelator was 0.5 wt% in all supramolecular gels.

POM: A blob of LC or hot LC sol was dripped on a glass, and then another glass was lidded with a certain amount of stress to fabricate the LC cell. The LC cell was investigated by POM.

Tube inversion method: The tube inversion method was used to measure the sol-gel transition temperature $T_{\text{sol-gel}}$. The test tube filled with LC physical gel was gently heated in an oil bath at 1°Cmin^{-1} , and $T_{\text{sol-gel}}$ was recorded when the gel was inverted. The measurement was repeated three times to acquire a mean value.

SEM measurements: A Hitachi S-4700 field emission scanning electron microscope (FESEM, Hitachi, Japan) was used to study microscopic morphology. Xerogel samples were sputtered with gold before SEM measurements.

Dynamic rheological measurements: A controlled-stress rheometer (MCR302, Anton Paar, Austria) was used to record the dynamic rheological measurements. The LC gels were coated onto the parallel-plate (25 mm diameter) with a gap of 1 mm and made steady for a certain time before testing. Dynamic frequency sweep tests were performed under a strain $\gamma=0.1\%$ with increasing frequency from 0.1 to 100 rad s^{-1} at 25°C .

XRD: An X-ray diffractometer (X’Pert PRO, PANalytical, Holland) with $\text{CuK}\alpha$ radiation ($\lambda=1.54\text{ \AA}$) was used to record the XRD frac-

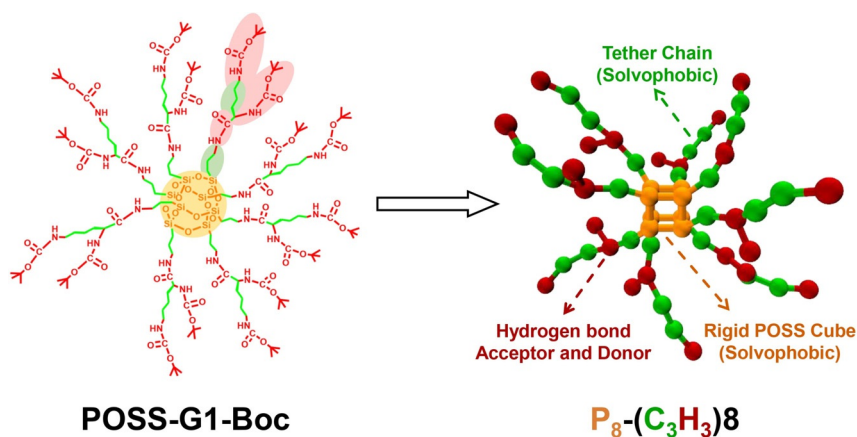


Figure 9. Coarse-grained model of POSS-G1-Boc, denoted as $P_8-(C_3H_3)_8$.

tion patterns of LC gels. It was performed at a filament current of 35 mA and with a voltage of 40 kV. The spectra were recorded in the 2θ range of $2-40^\circ$, at a scanning rate of $10^\circ \text{ min}^{-1}$.

E_T^N measurements: Reichardt's dye (RD) was used to test the normalized Reichardt's parameter E_T^N . An appropriate concentration of acetone solution of RD was added to LCs, respectively, and mixed adequately. The mixed reagents were dried under vacuum for 2 h to remove the acetone. Then the UV/Vis spectra of the samples were recorded to identify the wavelength of maximum absorption (λ_{max}). E_T^N was calculated from Equation (1).^[30]

Coarse-grained model: POSS-G1-Boc in the experiments was modeled as a coarse-grained molecule $P_8-(C_3H_3)_8$ (Figure 9). P (orange bead), C (green bead) and H (red bead) represent the POSS cube, the tether carbon chain, and the functional group that can form the hydrogen bond, respectively. According to the molecular configuration of POSS-G1-Boc and the relative length between POSS core and tethered chains, we chose suitable bead numbers for each segment (i.e., the subscripts in $P_8-(C_3H_3)_8$). Note that the POSS cube is generally treated as a rigid cube without distortion, and eight chains were tethered at the vertexes. All the neighboring beads are connected in the model by bonds with a harmonic spring potential. Angle bending potential was also introduced into this model to describe the branched angle in the tethered chains.

Molecular dynamic simulation: Different potential functions were introduced into the interaction between the pair of beads to realize the solvophobic nature and the hydrogen bonds of POSS-G1-Boc. The hydrogen-bond interaction between H beads (i.e., H-H interaction) was described by an acceptor-hydrogen-donor (AHD) three-body interaction potential from the DREIDING force field [Eq. (3)].^[32]

$$U_{\text{LJ}}^{\text{hb}} = \begin{cases} k_A (20r_{\text{AD}}^{-12} - 24r_{\text{AD}}^{-10}) \cos^4 \theta & \text{for } r_{\text{AD}} < R_c, \theta_{\text{AHD}} > \theta_c \\ 0 & \text{else} \end{cases} \quad (3)$$

in which k_A , R_c and θ_c are the force coefficient, cutoff distance, and cutoff angle, respectively. θ_{AHD} is the bond angle for acceptor-hydrogen-donor (AHD) three-body, while r_{AD} is the radial distance between donor and acceptor. The strength and the directivity of hydrogen-bond interaction are determined by k_A and θ_c , respectively.^[32,33] In this work, k_A , R_c and θ_c are set as 10ϵ , 5.0σ , and 150° , respectively, in which ϵ and σ are the unit of energy and length in the simulation. In addition, the standard Lennard-Jones (LJ) potential was chosen to describe the other pairwise interactions U_{ij} [Eq. (4)].^[34,35]

$$U_{ij} = \begin{cases} 4\epsilon_{ij} \left[\left(\frac{\sigma}{r_{ij}} \right)^{12} - \left(\frac{\sigma}{r_{ij}} \right)^6 - \left(\frac{\sigma}{r_{ij}} \right)^{12} + \left(\frac{\sigma}{r_{ij}} \right)^6 \right], & r \leq r_{ij}^c \\ 0, & r > r_{ij}^c \end{cases} \quad (4)$$

in which ϵ_{ij} and r_{ij} are the interaction strength and the radial distance between beads i and j . r_{ij}^c is the cutoff distance of LJ potential. For the P-P and C-C pairwise interactions, the attractive interaction was given by setting r_{ij}^c as 2.5σ due to the aggregation behavior of solvophobic POSS cube and tethered chain in a polar solvent. For the P-C, C-H and P-H pairwise interactions, the pure repulsion interaction was given by setting r_{ij}^c as $2^{1/6}\sigma$ to describe the incompatibility between different segments.

All the simulations were carried out using a Brownian Dynamic algorithm with the temperature controlling method (NVT ensemble).^[34,35] The simulations were performed by applying the simulator, coarse grained molecular dynamics program based on LAMMPS.^[36] Periodic boundary conditions were imposed. The integration time step $\Delta t = 0.005\tau$, and the simulation temperature $k_B T = 3.0\epsilon$ were selected, where τ was the unit of time in the simulation. Other Brownian dynamic simulation conditions can be found in our previous work.^[37,38]

Acknowledgements

This work was supported by the National Natural Science Foundation of China (grant no. 51773180) and College Student's Science and Technology Innovation Activity Plan of Zhejiang Province (Xinmiao Talent Project) (grant no. 2018R403086).

Conflict of interest

The authors declare no conflict of interest.

Keywords: molecular modeling • nanostructures • self-assembly • solvent effects • supramolecular chemistry

- [1] G. Palui, A. Banerjee, *J. Phys. Chem. B* **2008**, *112*, 10107–10115.
- [2] G. Kuang, Y. Ji, X. Jia, E. Chen, M. Gao, J. Yeh, Y. Wei, *Chem. Mater.* **2009**, *21*, 456–462.
- [3] S. Qu, L. Zhao, Z. Yu, Z. Xiu, C. Zhao, P. Zhang, B. Long, M. Li, *Langmuir* **2009**, *25*, 1713–1717.

- [4] X. Tong, Y. Zhao, B. K. An, S. Y. Park, *Adv. Funct. Mater.* **2006**, *16*, 1799–1804.
- [5] X. Tong, Y. Zhao, *J. Am. Chem. Soc.* **2007**, *129*, 6372–6373.
- [6] N. Mizoshita, Y. Suzuki, K. Hanabusa, T. Kato, *Adv. Mater.* **2005**, *17*, 692–696.
- [7] M. Moriyama, N. Mizoshita, T. Yokota, K. Kishimoto, T. Kato, *Adv. Mater.* **2003**, *15*, 1335–1338.
- [8] N. Mizoshita, T. Kato, *Adv. Funct. Mater.* **2006**, *16*, 2218–2224.
- [9] T. Kitamura, S. Nakaso, N. Mizoshita, Y. Tochigi, T. Shimomura, M. Moriyama, K. Ito, T. Kato, *J. Am. Chem. Soc.* **2005**, *127*, 14769–14775.
- [10] K. Yabuuchi, Y. Tochigi, N. Mizoshita, K. Hanabusa, T. Kato, *Tetrahedron* **2007**, *63*, 7358–7365.
- [11] J. He, B. Yan, B. Yu, R. Bao, X. Wang, Y. Wang, *J. Colloid Interface Sci.* **2007**, *316*, 825–830.
- [12] M. Andreis, D. Caric, N. S. Vujcic, M. Jokic, M. Zinic, M. Kveder, *Chem. Phys.* **2012**, *403*, 81–88.
- [13] S. Bi, H. Peng, S. Long, M. Ni, Y. Liao, Y. Yang, Z. Xue, X. Xie, *Soft Matter* **2013**, *9*, 7718–7725.
- [14] T. Kato, Y. Hirai, S. Nakaso, M. Moriyama, *Chem. Soc. Rev.* **2007**, *36*, 1857–1867.
- [15] Q. Jin, L. Zhang, M. Liu, *Chem. Eur. J.* **2013**, *19*, 9234–9241.
- [16] V. Čaplar, L. Frkanec, N. Šijacković Vujčić, M. Žinić, *Chem. Eur. J.* **2010**, *16*, 3066–3082.
- [17] M. Bielejewski, A. Lapinski, R. Luboradzki, J. Tritt-Goc, *Langmuir* **2009**, *25*, 8274–8279.
- [18] X. Ran, P. Zhang, S. Qu, H. Wang, B. Bai, H. Liu, C. Zhao, M. Li, *Langmuir* **2011**, *27*, 3945–3951.
- [19] M. L. Muro-Small, J. Chen, A. J. McNeil, *Langmuir* **2011**, *27*, 13248–13253.
- [20] P. Xue, Y. Zhang, J. Jia, D. Xu, X. Zhang, X. Liu, H. Zhou, P. Zhang, R. Lu, M. Takafuji, H. Ihara, *Soft Matter* **2011**, *7*, 8296–8304.
- [21] W. Edwards, C. A. Lagadec, D. K. Smith, *Soft Matter* **2011**, *7*, 110–117.
- [22] M. Bielejewski, A. Lapinski, R. Luboradzki, J. Tritt-Goc, *Tetrahedron* **2011**, *67*, 7222–7230.
- [23] G. Tang, S. Chen, F. Ye, X. Xu, J. Fang, X. Wang, *Chem. Commun.* **2014**, *50*, 7180–7183.
- [24] S. Chen, H. He, G. Tang, B. Wu, M. Ma, Y. Shi, X. Wang, *RSC Adv.* **2015**, *5*, 101437–101443.
- [25] S. Chen, X. Tong, H. He, M. Ma, Y. Shi, X. Wang, *ACS Appl. Mater. Interfaces* **2017**, *9*, 11924–11932.
- [26] S. Chen, Z. An, X. Tong, Y. Chen, M. Ma, Y. Shi, X. Wang, *Langmuir* **2017**, *33*, 14389–14395.
- [27] N. M. Sangeetha, U. Maitra, *Chem. Soc. Rev.* **2005**, *34*, 821–836.
- [28] L. A. Estroff, A. D. Hamilton, *Chem. Rev.* **2004**, *104*, 1201–1218.
- [29] S. Leiras, F. Freire, E. Quinoa, R. Riguera, *Chem. Sci.* **2014**, *6*, 246–253.
- [30] P. G. Jessop, D. A. Jessop, D. Fu, L. Phan, *Green Chem.* **2012**, *14*, 1245–1212.
- [31] V. Crescenzi, P. J. Flory, *J. Am. Chem. Soc.* **1964**, *86*, 141–146.
- [32] S. L. Mayo, B. D. Olafson, W. A. Goddard, *J. Phys. Chem.* **1990**, *94*, 8897–8909.
- [33] P. Xu, J. Lin, L. Zhang, *Phys. Chem. Chem. Phys.* **2018**, *20*, 15995–16004.
- [34] G. S. Grest, K. Kremer, *Phys. Rev. A* **1986**, *33*, 3628–3631.
- [35] M. A. Horsch, Z. Zhang, S. C. Glotzer, *Phys. Rev. Lett.* **2005**, *95*, 056105.
- [36] LAMMPS home page. <http://lammps.sandia.gov>.
- [37] S. Lin, N. Numasawa, T. Nose, J. Lin, *Macromolecules* **2007**, *40*, 1684–1692.
- [38] C. Yang, L. Gao, J. Lin, L. Wang, C. Cai, Y. Wei, Z. Li, *Angew. Chem. Int. Ed.* **2017**, *56*, 5546–5550; *Angew. Chem.* **2017**, *129*, 5638–5642.

 Manuscript received: March 26, 2019

Revised manuscript received: July 2, 2019

Accepted manuscript online: July 6, 2019

Version of record online: August 23, 2019